

Atomically Resolved Mapping of Polarization and Electric Fields Across Ferroelectric/Oxide Interfaces by Z-contrast Imaging

Hye Jung Chang, Sergei V. Kalinin, Anna N. Morozovska, Mark Huijben, Ying-Hao Chu, Pu Yu, Ramamoorthy Ramesh, Evgeny A. Eliseev, George S. Svechnikov, Stephen J. Pennycook, and Albina Y. Borisevich*

Polarization dynamics at the ferroelectric-metal interfaces is the dominant factor underpinning the functionality of ferroelectric devices including capacitors,^[1,2] direct probe-based data storage,^[3] field-effect transistors,^[4,5] and tunneling barriers.^[6–9] In particular, multiple theoretical studies have addressed the role of mesoscopic space-charge layers,^[10] non-uniform polarization distributions,^[11] and chemical bonding.^[12] Gerra et al.^[13] have shown theoretically that the planar corrugations responsible for the dipole moment can propagate from the ferroelectric to the oxide component, effectively smearing the distribution of polarization bound charge. Tsymbal et al.^[14,15] have demonstrated the role of interface bonding on dipole formation, painting a complex picture of multiple charge and polarization driven interactions even at nominally simple interfaces. Pruneda et al.^[16] have also demonstrated that ferrodistorive cation off-centering can arise near the surfaces of metallic oxides.

However, despite the multitude of mesoscopic studies based on Landau-Ginsburg-Devonshire (LGD) theory^[17,18] and density functional calculations,^[19,20] experimental studies of the polarization and field behavior at ferroelectric-metal interfaces have been much more limited. Jia et al.^[21,22] demonstrated the direct mapping of polarization fields in the vicinity of domain walls and interfaces using phase contrast imaging (parallel electron

beam) in the aberration-corrected transmission electron microscope. On the nanometer scales, electron holography has been used to extract potential and charge distributions.^[23] In this work, we utilize Z-contrast imaging in aberration-corrected scanning transmission electron microscopy (STEM, using convergent electron beam) to map the atomic structure and polarization across the interface at the atomic level. We compare two polarization orientations of BiFeO₃/(La_xSr_{1-x})MnO₃ interfaces, which, through LGD analysis, allows us to separate the contributions of interface charge from polarization charge at the interface, and extract a complete description of the electrostatic field distribution across the heterostructure with atomic resolution.

For our studies, we use multiferroic BiFeO₃ (BFO) that offers the advantage of relatively large atomic displacements that can be directly detected by Z-contrast STEM. Films were grown on a (100) SrTiO₃ (STO) substrate with a 5 nm-thick ferromagnetic La_{0.7}Sr_{0.3}MnO₃ (LSMO) electrode, as described previously.^[24,25] **Figure 1a** shows a high angle annular dark field (HAADF) image of a 4.8 nm BFO/LSMO/STO thin film in [100] pseudocubic orientation. The image shows clear contrast of the LSMO and BFO components suggesting that the interface is sharp. There is no detectable change in the lattice parameter parallel to the interface. No defects such as misfit dislocations were observed anywhere in the sample. Atomic-resolution electron energy loss spectroscopy (EELS) line scans are presented in **Figure 1b**. The intensity profiles for La, Mn, Fe and Ti show well-defined transitions with a width of about two unit cells at each interface, confirming that the interface is indeed sharp. The small finite width can be attributed to beam spreading through the thickness of the sample.

We observe the polarization down the [110] pseudocubic axis, as it affords the best alignment between the polarization direction and image plane. **Figure 2a** demonstrates the quantification process schematically. The positions of Bi and Fe ions in the unit cell are determined from the raw image by statistical methods; the difference in the *z* and *y* positions of the Fe cations from the midpoint between Bi cations is interpreted as ferroelectric displacement. The associated error can be estimated from the changes in extracted polarization parallel to the interface in the absence of defects. In the original quantification method developed by Jia et al.,^[21,22] it is required to map all three sublattices, including oxygen, to calculate the value of polarization. However, it has been shown theoretically that in bismuth ferrite (unlike Pb(Zr,Ti)O₃ examined by Jia et al.), the

Dr. H. J. Chang, Dr. S. V. Kalinin, Dr. S. J. Pennycook, Dr. A. Borisevich
Oak Ridge National Laboratory
Oak Ridge, Tennessee 37831, USA
E-mail: albinab@ornl.gov

Dr. A. N. Morozovska, Dr. E. A. Eliseev, Prof. G. S. Svechnikov
V. Lashkarev Institute of Semiconductor Physics
NAS of Ukraine, 41, pr. Nauki, 03028 Kiev, Ukraine

Dr. M. Huijben
Faculty of Science and Technology
MESA + Institute for Nanotechnology
University of Twente
P.O. BOX 217, 7500 AE, Enschede, The Netherlands

Dr. M. Huijben, P. Yu, Prof. R. Ramesh
Department of Materials Science and Engineering
and Department of Physics
University of California
Berkeley, California, 94720, USA

Prof. Y.-H. Chu
Department of Materials Science and Engineering
National Chiao Tung University
Hsinchu, Taiwan 30013, ROC

DOI: 10.1002/adma.201004641

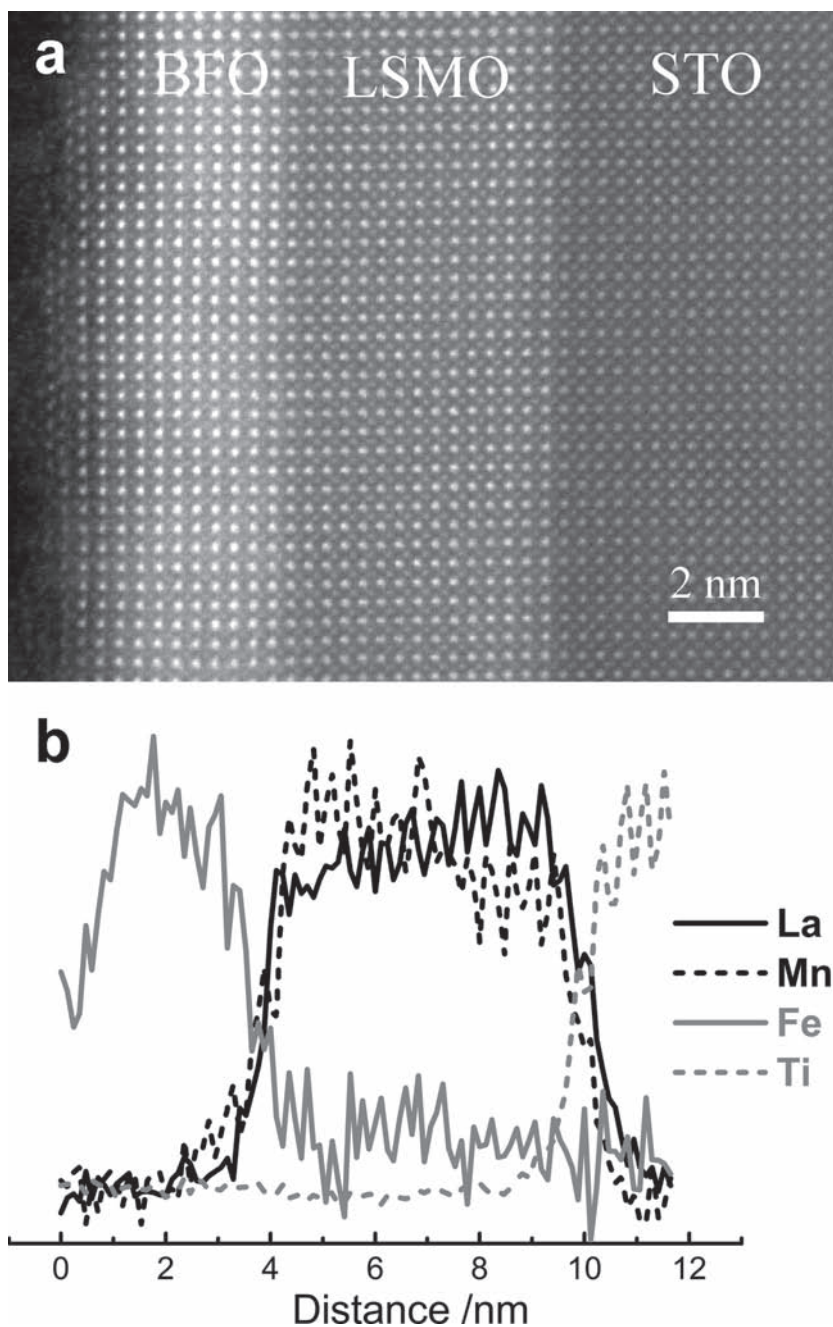


Figure 1. (a) HAADF STEM image of the 3.2 nm BFO/5 nm LSMO/STO multilayer structure in 100. orientation; (b) intensities calculated from EELS line scan for La (black solid), Mn (black dash), Fe (gray solid), and Ti (gray dash) across the interface. Note periodic peaks on the profiles corresponding to atomic columns. Profile transition widths at the interfaces are about 2 unit cells (see text).

Fe displacement relative to Bi is the dominant manifestation of ferroelectric polarization and stays dominant under epitaxial strain.^[26,20] As a result, bright field STEM imaging for mapping oxygen positions is not required in this case, allowing the use of relatively thick (up to 50–100 nm) samples. The use of thick samples offers the additional advantage of avoiding depolarization field effects on ferroelectric phase stability, which can be significant for thicknesses less than 5 nm as often reported for

high resolution TEM. For thinner samples, we have also studied oxygen positions in the vicinity of the interface, but found that those were not correlated to sample thickness or polarization direction. Those results are reported elsewhere.^[27]

Figure 2b and f show the portions of the HAADF STEM images of (thin) 50 nm and (ultrathin) 3.2 nm BFO films, respectively, which were analyzed using the approach illustrated in Figure 2a. Figure 2g and h show two-dimensional maps of Fe displacement in both z (normal to the interface, Figure 2g) and y (along the interface, Figure 2h) directions measured for the ultrathin film (Figure 2f). The graph averaging the displacements over 12 rows parallel to the interface is given in Figure 2i. We can see that there is no measurable y displacement in this case, implying the [001] rhombohedral orientation of BFO (with in-plane polarization collinear with electron beam) or possibly tetragonal structure as suggested by Bea et al.^[28] The polarization behavior at the interface (apparently) follows the model predicted by Tagantsev^[12] – i.e., a virtually uniform polarization distribution within the ferroelectric component, an abrupt polarization change at the BFO/LSMO interface, and a gradual decay of induced polarization inside the oxide metal (of the same sign as in the ferroelectric), such that Mn atoms in the 6 rows nearest the interface also exhibit small off-center negative displacements.

A similar plot for the thicker (50 nm) film (Figure 2b), averaging the displacements over six atomic rows, is presented in Figure 2e, with the 2D displacement maps given in Figure 2c (z , component normal to the interface) and 2d (y , component along the interface). Note that the z displacement is positive, while the y displacement is negative. We can see that magnitudes of the two displacements are comparable, with the direction normal to the interface (in this case, towards it) slightly larger. This displacement pattern implies that the BFO must be in the $[10\bar{1}]$ rhombohedral orientation. Unlike the thin film, the polarization decays gradually over the last four BFO atomic layers toward the interface; the decline is gradual for both in-plane and out-of-plane components of polarization. Here, we focus on the out-of-plane (z) displacement component, since it is the polarization projection on the interface normal that results in bound charge. It can be seen from Figure 2e that after crossing the interface into LSMO, the z displacement briefly switches sign, which implies that Mn atoms in the first few rows are slightly displaced towards the interface from the other side. Hence, this behavior does not follow the Tagantsev^[12] prediction. The polarization in the

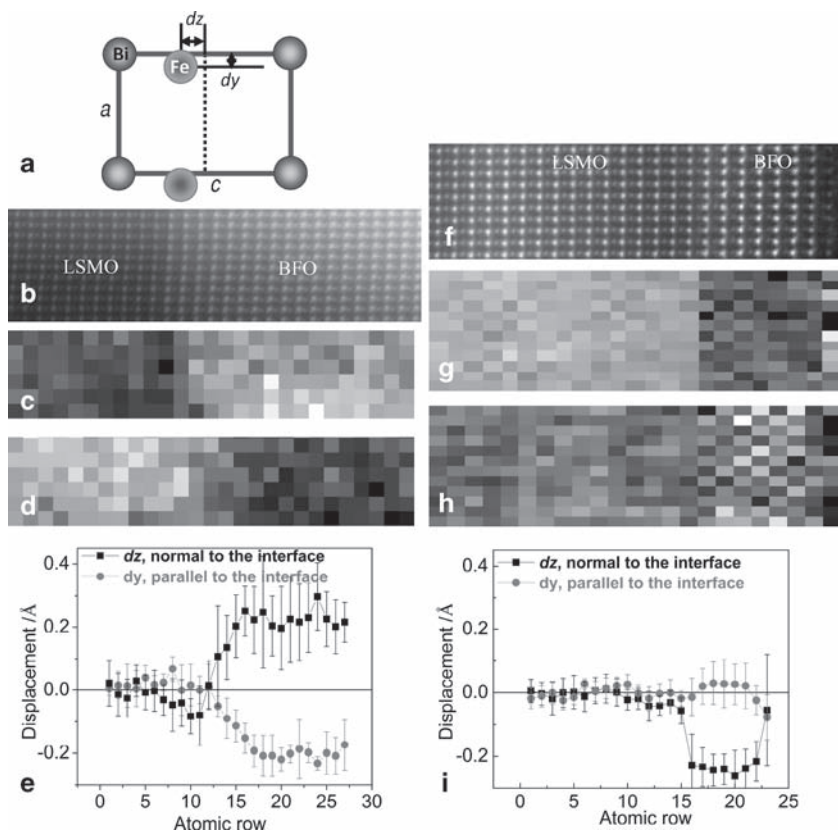


Figure 2. HAADF STEM studies of STO-LSMO-BFO multilayers. (a) Schematic of the displacement quantification in $(110)_c$ oriented bismuth ferrite; (b) HAADF STEM image of the STO/5 nm LSMO/50 nm BFO thin film; (c,d) the corresponding 2D displacement maps for z and y directions, respectively; (e) line plots obtained by averaging the data in (c,d) along the interface; (f) HAADF STEM image of the STO/5 nm LSMO/3.2 nm BFO thin film; (g,h) the corresponding 2D displacement maps for z and y directions, respectively; (i) line plots obtained by averaging the data in (g,h) along the interface.

BFO layer is no longer constant, but rather illustrates a gradual decay over 3–5 unit cells towards the interface, with essentially zero polarization at the interface.

Overall, the polarization in the LSMO shows the same sign, magnitude and spatial extent as in the case of the thin film. This polarization behavior is consistent with the presence of a frozen polarization component in the LSMO and/or fixed interface charge or specific chemical bonding at the LSMO/BFO interface. Similar behavior was recently theoretically predicted by Tsymbal for ferroelectric interfaces.^[14,15] The origin of this behavior is most likely due to the interface charge mismatch, where the difference in the valence states between the adjacent layers will give rise to a formal charge of -0.3 e per unit cell for $(\text{La}_{0.7}\text{Sr}_{0.3}\text{O})/(\text{FeO})$ termination or $+0.3$ e per unit cell for $(\text{MnO}_2)/(\text{BiO})$ termination. The interface stacking is ambiguous from Figure 1B, so that both terminations may coexist. In addition we cannot exclude specific chemical bonding or oxygen vacancy gradients formed during deposition from contributing to the interface charge.

For a thin film where the polarization partially compensates the interfacial charge, a sharp interface is expected, whereas for antiparallel orientation, a broad “charged” interface is expected, exactly as we observe. Note that the interface contribution is

independent of film thickness, whereas the bulk contribution is linear in film thickness. This consideration rationalizes the preferential formation of a stable interface in the thin film, where the film has switched polarization to minimize interfacial energy. In contrast, in the thick film the bulk polarization state is controlled by the built-in field in the ferroelectric, and the interfacial region is wider.

Next we quantify the electrostatic behavior of the interface as a function of polarization by employing the mesoscopic model based on solution of the Landau–Ginzburg–Devonshire (LGD) equation for semiconductor–ferroelectric junction. While it can be expected that studies of the electric field distribution on the atomic level require density-functional theory based models, recent analysis of polarization dynamics in ferroelectric multilayers^[29] illustrates that for thicknesses of several unit cells mesoscopic models yield results close to density-functional theory. Combined with the fact that the observed displacement patterns are relatively smooth on the level of several unit cells, this suggests that mesoscopic theory will be applicable here.

We determine the polarization and field distribution in a ferroelectric film of thickness L in contact with a semiconductor electrode, shown schematically in Figure 3a. The counter electrode is provided by surface states screening, described as an effective metal electrode. Hence, the heterostructure consists of metal electrode, ferroelectric-dielectric film of thickness L that interfaces at $z = 0$ with the semiconductor at $z < 0$. The contact

potential difference U_b appears at the contact $z = 0$ (see inset in Figure 3). External bias is absent. The surface band bending (or intrinsic field effect) originating in the semiconductor leads to a depletion (or accumulation) layer of thickness W with space charge density charge ρ .^[30] The interface charge σ_s located at $z = 0$ modifies the Schottky barrier.^[31,32] Subsequently, we solve Maxwell’s equations $\epsilon_0 \epsilon_{33}^b (\partial^2 \varphi / \partial z^2) = \partial P_3 / \partial z$ (at $-L < z < 0$) and $\epsilon_0 \epsilon_s (\partial^2 \varphi / \partial z^2) = -\rho$ (at $z > 0$) for the quasi-static electric field $\mathbf{E} = -\nabla \varphi(z)$. The boundary conditions at $z = -L$, $z = 0$ and $z = +\infty$, are $\varphi(x, y, L) = 0$, $D_3(z < L) = 0$, $\varphi(x, y, +0) - \varphi(x, y, -0) = U_b$, $D_3(x, y, -0) - D_3(x, y, +0) = \sigma_s$, $\varphi(x, y, z \rightarrow \infty) = 0$.

In the depletion layer approximation analytical expressions are obtained as follows,

$$E_3(z) \approx -\frac{P_3(z)}{\epsilon_0 \epsilon_{33}^b} + \frac{\rho W - \sigma_s}{\epsilon_0 \epsilon_{33}^b}, \text{ at } 0 < z < L,$$

$$E_3(z) = \frac{\rho(z+W)}{\epsilon_0 \epsilon_s} \theta(z+W), \text{ at } z < 0. \quad (1)$$

where $\theta(z)$ is the Heaviside step-function, ϵ_{33}^b is the dielectric permittivity of the reference state,^[33] ϵ_s is the semiconductor (bare) lattice permittivity, ϵ_0 is the universal dielectric constant.

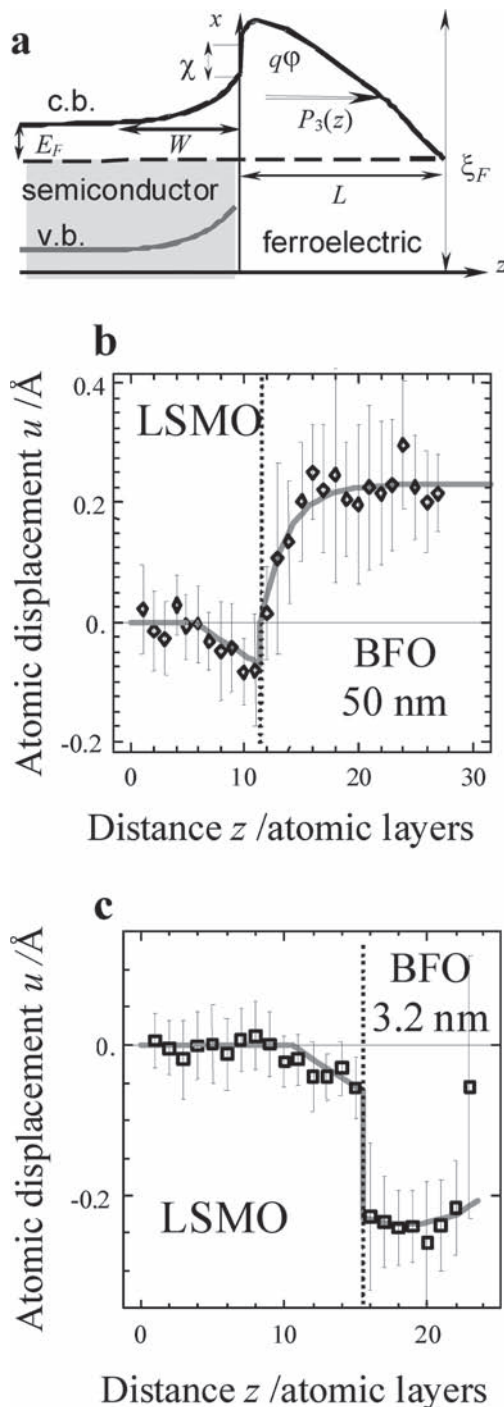


Figure 3. (a) Schematic band structure for a half-metal-ferroelectric-metal system with key parameters: P_3 is ferroelectric polarization, A_m is the work function, ϕ is electrostatic potential, χ is electron affinity, ξ_F is Fermi level, q is elementary charge, c.b. is the conduction band, v.b. is the valence band. (b, c) Atomic displacement distribution inside the LSMO/BFO structure having a BFO film thickness of (b) 125 l.c. and (c) 8 l.c. Symbols with error bars represents experimental results, solid curves are calculated from Equations 1–5 for the following parameters: $U_b = 0.7$ V, $P_b = 0$, (b) $L = 125$ l.c., $W = 6.06$ l.c., $\lambda_1 = 0$, $\lambda_2 = 5$ l.c., $\langle P_3 \rangle = 0.24$ C/m² and $\sigma_S = 0.35$ C/m². (c) $L = 8$ l.c., $W = 6.17$ l.c., $\lambda_1 = 37.5$ l.c., $\lambda_2 = 12.5$ l.c., $\langle P_3 \rangle = -0.24$ C/m² and $\sigma_S = -0.15$ C/m². Other parameters are listed in the Tables 1–2 of the Supporting Information.

The polarization distribution $P_3(z)$ was then found from the Euler-Lagrange boundary problem:

$$\begin{cases} \alpha(T)P_3 + \beta P_3^3 + \gamma P_3^5 - g \frac{d^2 P_3}{dz^2} = E_3(z), \\ (P_3 + \lambda_1 \frac{dP_3}{dz})|_{z=0} = -P_b, (P_3 - \lambda_2 \frac{dP_3}{dz})|_{z=L} = 0. \end{cases} \quad (2)$$

The distance across the interface is z (Figure 3a). Here $\lambda_{1,2}$ are extrapolation lengths, the LGD free energy expansion coefficients $\beta < 0$ for the first order ferroelectrics, $\gamma > 0$ and the gradient term $g > 0$. The coefficient $\alpha(T) = \alpha_T (T - T_c^*)$, where T is the absolute temperature. T_c^* is the Curie temperature renormalized by the epitaxial misfit strain $u_m = (a/c) - 1$.

The inhomogeneity P_b represents the interface polarization that produces an interface dipole.^[14,15] More generally, the translational symmetry breaking that is inevitably present at any interface gives rise to the inhomogeneity in the boundary conditions (2).^[34,35] Using a modified direct variational method,^[36] an approximate analytical solution of Equation 2 was derived as summarized in Appendix A. Estimation for LSMO material parameters of $\rho = eN$, where the carrier concentration $N = (0.5-2) \times 10^{27}$ m⁻³,^[37,38] $\epsilon_S = 20-30$,^[39] BFO polarization $\langle P_3 \rangle = 0.5-1$ C/m², $\epsilon_{33}^b \sim 10$ and $L \sim 10^{-9} - 10^{-7}$ m leads to $W = 1-8$ nm.

Equation 2 can be used to describe polarization patterns in Figure 2 directly, enabling the associated parameters to be extracted. The atomic displacement $\mathbf{u} = \sum_j \mathbf{r}_j - \mathbf{R}_m$ measured in the inertial reference frame is regarded as related to the unit cell dipole moment $\mathbf{d} = \mathbf{P}V_{cell} = \sum_j q_j \mathbf{r}_j$ and acquires the form $u_3^{F,E,S}(z) \approx P_3(z) V_{F,E,S} / q_{F,E,S}^B$, where V_j is the volume of the corresponding unit cell, q^B is the effective Born charge of the lightest atom “B”, and $\sum_j q_j = 0$ for a unit cell. The approximate expression is valid until $\sum_{n \neq B} m_n \gg m_B$. The vertical atomic displacement was fitted to experimental data with the help of a self-consistent procedure, such that σ_S and ϵ_{33}^b were determined (see Figure 3b,c).

After extracting the interface parameters, we can reconstruct the polarization P_3 , field E_3 and space charge in the LSMO/BFO heterostructures as shown in Figure 4. It is clear from Figure 4a,b that the polarization z -distribution is proportional to atomic displacement shown in Figure 3b and c as anticipated. We can also calculate the electrical displacement z -distribution from Equation 1 as $D_3 = P_3 + \epsilon_0 E_3$, which is linear inside the semiconducting LSMO and constant inside the ferroelectric BFO. The displacement jump at the LSMO/BFO interface $z = 0$ originates from interface charges with positive density $\sigma_S = 0.35$ C/m² (0.33 e per unit cell area) for the 50 nm BFO film and negative density $\sigma_S = -0.15$ C/m² (-0.14 e per unit cell area) for the 3 nm BFO film. The interface charges also facilitate spontaneous polarization screening. Hence, the different signs of the charge σ_S correspond to the different polarization orientation for the two cases considered. Note that it was impossible to fit the experimental data using $\sigma_S = 0$, even using high P_b values for both films. The absence of surface charge ($\sigma_S = 0$) leads to a drastic drop of polarization in thin films due to the poor screening of spontaneous polarization by the bulk charge in the semiconductor. The surface charges σ_S provide much more effective screening of spontaneous polarization and thus increase the P_3 value self-consistently. Close values of $W \approx 6$ lattice constants (l.c.) for both orientations of polarization is consistent with the appearance of interface charges, since in their

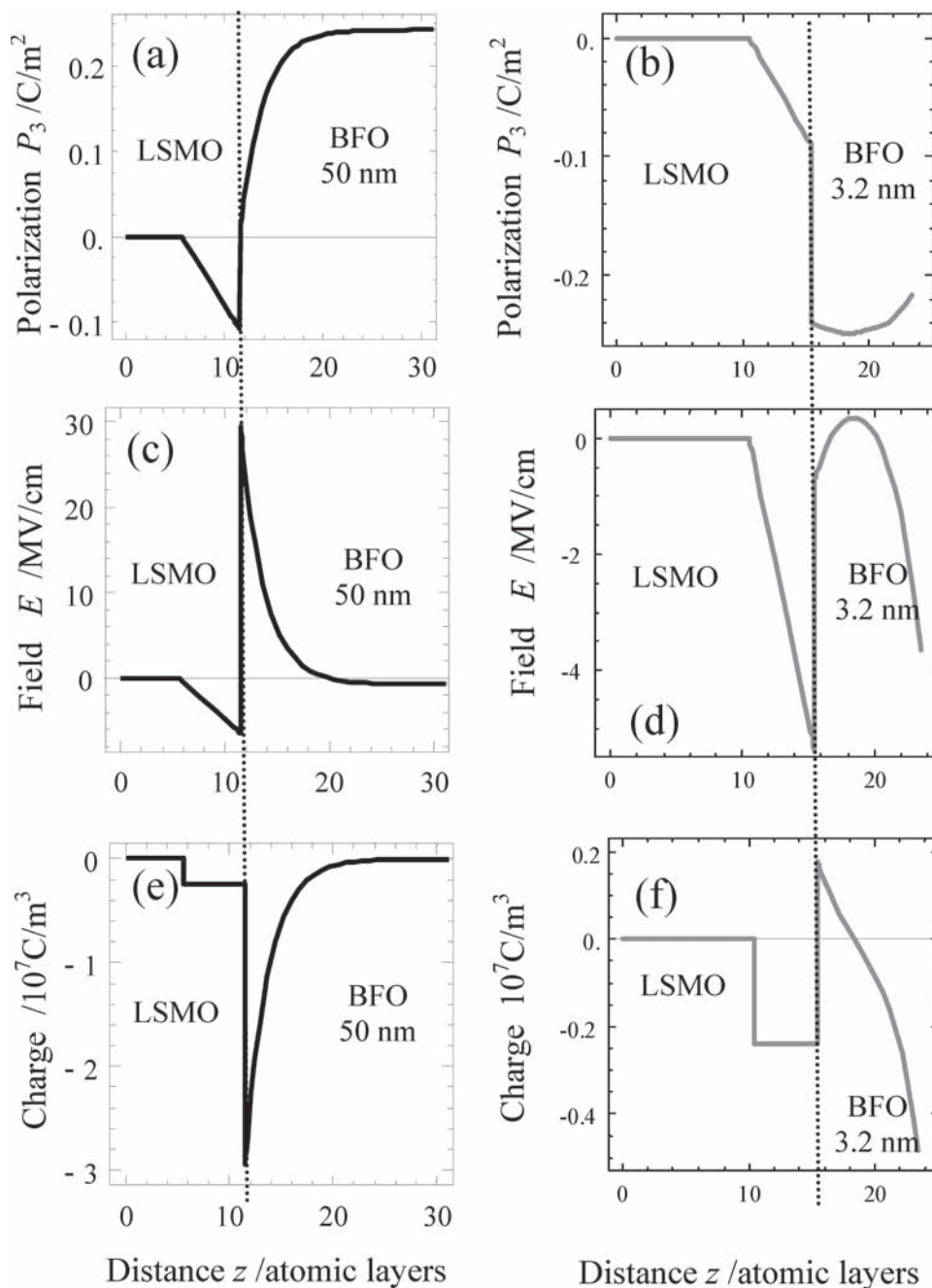


Figure 4. (a,b) Polarization, (c,d) electric field, and (e,f) space charge (bound and free) z -distributions inside the LSMO/BFO heterostructure (a,c) for the BFO film of 125 $l.c.$ and (b,d) 8 $l.c.$ for the same parameters as in Figure 2b,c.

absence ($\sigma_s = 0$), “bulk” screening would give different values of W in the different polarization directions. Actually for the case of purely “bulk” screening the bound charges of different sign are screened by the minor (n-type) and major (p-type) carriers with strongly different concentration in the improper semiconductor (p-type LSMO).

The complete potential distribution ϕ inside the LSMO/BFO heterostructure can also be reconstructed from the fitting of experimental data shown in Figure 3 (see Supporting Information).

To summarize, we used direct structural imaging using aberration-corrected STEM to map polarization fields at the BFO-LSMO interface. In the thicker film, the polarization is found to decay within the ferroelectric phase over 3–5 unit cells and is essentially zero at the interface. In the LSMO phase, the formation of a polarized layer opposite to the BFO polarization is observed. Hence, the interface forms an effective head-to-head domain wall. In contrast, in the thin film the polarization in the ferroelectric phase and LSMO are collinear, and the interface

is formed by a stable head-to-tail arrangement. These observations are consistent with strong interface polarization pinning at the BFO-LSMO interface. This frozen polarization will significantly affect the polarization switching in these systems and result in the presence of large interfacial fields. In particular, in thin LSMO the polarization is apparently controlled by the interface charge, and only weakly affected by the ferroelectric polarization of the film. Using modified LGD theory, we have then extracted the numerical values of interface and polarization charges at the interface from the experimental displacement profiles. Notably, the modeling results reinforce the suggestion of a pivotal role that interface charge (a.k.a. polar discontinuity) plays in the properties of these interfaces. In a more general perspective, these results show how electrostatic fields can be directly mapped in ferroelectric materials on the atomic level through the detection of associated structural distortions. This provides an alternative methodology to holography, which requires a thin film near a region of vacuum to allow interference between the transmitted and reference beams.

Supporting Information

Supporting Information is available from the Wiley Online Library or from the author.

Acknowledgements

Research sponsored by the Materials Sciences and Engineering Division of the US DOE, by Laboratory Directed Research and Development (LDRD) funding from Oak Ridge National Laboratory, and by appointment (H.J.C.) to the ORNL Postdoctoral Research Program administered jointly by ORNL and ORISE. AYB partially supported by ORNL's Shared Research Equipment (SHaRE) User Facility, which is sponsored by the Office of Basic Energy Sciences, U.S. Department of Energy. The Ukrainian group acknowledges Ministry of Science and Education of Ukraine (grant UU30/004) and NAS Ukraine and National Science Foundation (Materials World Network, DMR-0908718).

Received: December 17, 2010
Published online: April 29, 2011

- [1] A. K. Tagantsev, L. E. Cross, J. Fousek, *Domains in Ferroic Crystals and Thin Films*, Springer, 2010.
- [2] J. Scott, *Ferroelectric Memories*, Springer Verlag, Berlin 2000.
- [3] T. Tybell, C. H. Ahn, J.-M. Triscone, *Appl. Phys. Lett.* **1998**, *72*, 1454.
- [4] a) S. L. Miller, P. J. McWhorter, *J. Appl. Phys.* **1992**, *72*, 5999; b) S. L. Miller, P. J. McWhorter, *J. Appl. Phys.* **72**, 5999.
- [5] S. Mathews, R. Ramesh, T. Venkatesan, J. Benedetto, *Science* **1997**, *276*, 238.
- [6] E. Y. Tsymbal, H. Kohlstedt, *Science* **2006**, *313*, 181.
- [7] P. Maksymovych, S. Jesse, P. Yu, R. Ramesh, A. P. Baddorf, S. V. Kalinin, *Science* **2009**, *324*, 1421.
- [8] V. Garcia, S. Fusil, K. Bouzehouane, S. Enouz-Vedrenne, N. D. Mathur, A. Barthelemy, M. Bibes, *Nature* **2009**, *460*, 81.
- [9] A. Gruverman, D. Wu, H. Lu, Y. Wang, H. W. Jang, C. M. Folkman, M. Y. Zhuravlev, D. Felker, M. Rzchowski, C. B. Eom, E. Y. Tsymbal, *Nano Lett.* **2009**, *9*, 3539.
- [10] Y. Xiao, V. B. Shenoy, K. Bhattacharya, *Phys. Rev. Lett.* **2005**, *95*, 247603.
- [11] E. V. Chensky, V. V. Tarasenko, *Zh. Eksp. Teor. Fiz.* **1982**, *83*, 1089.
- [12] A. K. Tagantsev, G. Gerra, N. Setter, *Phys. Rev. B* **2008**, *77*, 174111.
- [13] G. Gerra, A. K. Tagantsev, N. Setter, *Phys. Rev. Lett.* **2007**, *98*, 207601.
- [14] C. G. Duan, R. F. Sabirianov, W. N. Mei, S. S. Jaswal, E. Y. Tsymbal, *Nano Lett.* **2006**, *6*, 483.
- [15] J. P. Velez, C. G. Duan, K. D. Belashchenko, S. S. Jaswal, E. Y. Tsymbal, *Phys. Rev. Lett.* **2007**, *98*, 137201.
- [16] J. M. Pruneda, V. Ferrari, R. Rurali, P. B. Littlewood, N. A. Spaldin, E. Artacho, *Phys. Rev. Lett.* **2007**, *99*, 226101.
- [17] Y. Watanabe, *Phys. Rev. B* **1998**, *57*, 789.
- [18] Y. Zheng, C. H. Woo, *Nanotechnology* **2009**, *20*, 075401.
- [19] M. Stengel, D. Vanderbilt, N. A. Spaldin, *Nat. Mater.* **2009**, *8*, 392.
- [20] A. Lubk, S. Gemming, N. A. Spaldin, *Phys. Rev. B* **2009**, *80*, 104110.
- [21] C. L. Jia, V. Nagarajan, J. Q. He, L. Houben, T. Zhao, R. Ramesh, K. Urban, R. Waser, *Nat. Mater.* **2007**, *6*, 64.
- [22] C. L. Jia, S. B. Mi, K. Urban, I. Vrejoiu, M. Alexe, D. Hesse, *Nat. Mater.* **2008**, *7*, 57.
- [23] H. Lichte, M. Reibold, K. Brand, M. Lehmann, *Ultramicroscopy* **2002**, *93*, 199.
- [24] M. Huijben, L. W. Martin, Y. H. Chu, M. B. Holcomb, P. Yu, G. Rijnders, D. H. A. Blank, R. Ramesh, *Phys. Rev. B* **2008**, *78*, 094413.
- [25] L. W. Martin, Y. H. Chu, M. B. Holcomb, M. Huijben, P. Yu, S. J. Han, D. Lee, S. X. Wang, R. Ramesh, *Nano Lett.* **2008**, *8*, 2050.
- [26] G. Catalan, J. F. Scott, *Adv. Mater.* **2009**, *21*, 2463.
- [27] A. Y. Borisevich, H. J. Chang, M. Huijben, M. P. Oxley, S. Okamoto, M. K. Niranjan, J. D. Burton, E. Y. Tsymbal, Y. H. Chu, P. Yu, R. Ramesh, S. V. Kalinin, S. J. Pennycook, *Phys. Rev. Lett.* **2010**, *105*, 087204.
- [28] H. Bea, M. Bibes, S. Petit, J. Kreisel, A. Barthelemy, *Philos. Mag. Lett.* **2007**, *87*, 165.
- [29] S. M. Nakhmanson, K. M. Rabe, D. Vanderbilt, *Phys. Rev. B* **2006**, *73*, 060101.
- [30] A. N. Morozovska, E. A. Eliseev, S. V. Svechnikov, A. D. Krutov, V. Y. Shur, A. Y. Borisevich, P. Maksymovych, S. V. Kalinin, *Phys. Rev. B* **2010**, *81*, 205308.
- [31] J. Bardeen, *Phys. Rev.* **1947**, *71*, 717.
- [32] V. M. Fridkin, *Ferroelectric Semiconductors*, Consultants Bureau, New York/London **1980**, p.119.
- [33] C. H. Woo, Y. Zheng, *Appl. Phys. A* **2008**, *91*, 59.
- [34] M. M. D. Glinchuk, A. N. Morozovska, *J. Phys. Cond. Matter* **2004**, *16*, 3517.
- [35] M. D. Glinchuk, A. N. Morozovska, E. A. Eliseev, *J. Appl. Phys.* **2006**, *99*.
- [36] E. A. Eliseev, A. N. Morozovska, *J. Mater. Sci.* **2009**, *44*, 5149.
- [37] A. Tiwari, C. Jin, D. Kumar, J. Narayan, *Appl. Phys. Lett.* **2003**, *83*, 1773.
- [38] A. Ruotolo, C. Y. Lam, W. F. Cheng, K. H. Wong, C. W. Leung, *Phys. Rev. B* **2007**, *76*, 075122.
- [39] J. L. Cohn, M. Peterca, J. J. Neumeier, *Phys. Rev. B* **2004**, *70*, 214433.